

Solitons in \mathcal{PT} -symmetric periodic systems with the quadratic nonlinearity

F. C. Moreira^{1,2}, V. V. Konotop², and B. A. Malomed³

¹*Universidade Federal de Alagoas, Campus A. C. Simões - Av. Lourival Melo Mota, s/n, Cidade Universitária, Maceió - AL 57072-900, Brazil*

²*Centro de Física Teórica e Computacional and Departamento de Física, Faculdade de Ciências, Universidade de Lisboa, Avenida Professor Gama Pinto 2, Lisboa 1649-003, Portugal and*

³*Department of Physical Electronics, School of Electrical Engineering, Faculty of Engineering, Tel Aviv University, Tel Aviv 69978, Israel*

(Dated: November 10, 2018)

We introduce a one-dimensional system combining the \mathcal{PT} -symmetric complex periodic potential and the $\chi^{(2)}$ (second-harmonic-generating) nonlinearity. The imaginary part of the potential, which represents spatially separated and mutually balanced gain and loss, affects only the fundamental-frequency (FF) wave, while the real potential acts on the second-harmonic (SH) component too. Soliton modes are constructed, and their stability is investigated (by means of the linearization and direct simulations) in semi-infinite and finite gaps in the corresponding spectrum, starting from the bifurcation which generates the solitons from edges of the gaps' edges. Families of solitons embedded into the continuous spectrum of the SH component are found too, and it is demonstrated that a part of the families of these *embedded solitons* (ESs) is stable. The analysis is focused on effects produced by the variation of the strength of the imaginary part of the potential, which is a specific characteristic of the \mathcal{PT} system. The consideration is performed chiefly for the most relevant case of matched real potentials acting on the FF and SH components. The case of the real potential acting solely on the FF component is briefly considered too.

PACS numbers: 42.65.Jx, 42.65.Tg, 42.65.Wi

I. INTRODUCTION

There is a growing interest in physical systems possessing the so-called \mathcal{PT} (parity-time) symmetry [1, 2], i.e., as a matter of fact, dissipative quantum systems with the antisymmetry between spatially separated gain and loss. If the strength of the gain-loss terms does not exceed a certain threshold value, the \mathcal{PT} -symmetric system has a purely real spectrum and its non-Hermitian Hamiltonians can be transformed into a Hermitian form [3]. Making use of the similarity of the quantum-mechanical Schrödinger equation to the parabolic propagation equation in optics it was proposed theoretically [4] and demonstrated experimentally [5] that the \mathcal{PT} symmetry can be realized, in the purely classical context of the wave propagation, in optics, where it implies that a waveguide with the \mathcal{PT} -balanced gain and losses allows the transmission of wave modes, emulating the index-guiding transmission in ordinary (conservative) waveguides. These findings stimulated numerous additional studies of the linear wave propagation in [2] \mathcal{PT} -symmetric systems with particular attention being focused on the periodic potentials [6] (see also review [7]).

Due to optical applications, additional interest has been recently attracted by nonlinear \mathcal{PT} -symmetric optical systems with periodic modulation of the refractive index [8] which demonstrated that stable solitons can be supported by the combination of the Kerr nonlinearity and periodic complex potentials, whose spatially odd imaginary part accounts for the balanced gain and loss. The stability of such solitons was rigorously analyzed in Ref. [9]. Solitons can also be naturally found in linearly-coupled dual-core systems with balanced gain and loss

in the two cores and intrinsic Kerr (cubic) nonlinearity in each one [10], and discrete solitons were predicted in coupled chains of \mathcal{PT} -symmetric elements [11] and in general network of coupled \mathcal{PT} -symmetric oligomers (dimers, quadrimers, etc) [12]. In addition to introducing the usual Kerr nonlinearity, the \mathcal{PT} -symmetric part of the system can be made nonlinear too, by introducing mutually balanced cubic gain and loss terms [13]. Properties of solitons in \mathcal{PT} systems may differ significantly from what is known about usual solitons in conservative models. In particular, different families of solutions bifurcating from different linear modes may merge in a single family, exhibiting increased stability [14]. On the other hand, the increase of the gain-loss coefficient in the \mathcal{PT} -symmetric Kerr-nonlinear coupler leads to shrinkage of the stability areas for \mathcal{PT} -symmetric and antisymmetric solitons, until they vanish when this coefficient becomes equal to the inter-core coupling constant. We also mention recent intensive activity in study of the combined effect of linear and nonlinear \mathcal{PT} [15] on existence and stability of optical solitons.

Apart from the Kerr nonlinearity, another fundamental type of nonlinear interactions in optical media is quadratic ($\chi^{(2)}$), which gives rise to the second-harmonic-generation systems, which generate families of two-color solitons, [16]. Recently the soliton dynamics in $\chi^{(2)}$ materials was considered in the presence of a \mathcal{PT} -symmetric localized impurity [17]. The objective of the present work is to introduce a generic one-dimensional (1D) system with the \mathcal{PT} -symmetric periodic complex potential and conservative $\chi^{(2)}$ nonlinearity, and construct stable solitons in it. The realization of such a system in the spatial domain is quite possible in optics,

using appropriately juxtaposed gain and loss elements, like in Ref. [5], inserted into a $\chi^{(2)}$ medium. We here focus on the search for gap solitons (GSs) in the system with the periodic potential, i.e., localized solutions whose propagation constant belongs to regions of the forbidden propagation (*gaps*) in the underlying linear spectra. Similarly to the usual $\chi^{(2)}$ systems (which do not include gain and loss) [16], the quadratic nature of the nonlinearity makes the interplay between the gaps of the fundamental-frequency (FF) and second-harmonic (SH) fields a fundamental factor affecting GS families. In particular, the generic mechanism of the creation of the families via bifurcations from edges of the bandgaps [18] can work in the FF or SH component, or in both [17]. We here analyze all these possibilities.

It is relevant to mention that, as the \mathcal{PT} -symmetric systems is a special type of settings at the border between conservative and dissipative systems, the solitons that exist in them may be naturally compared not only to their counterparts in conservative models (as mentioned above, concerning the relation to GSs in the conservative $\chi^{(2)}$ systems), but also to solitons in generic dissipative systems, with unbalanced gain and loss. The crucial difference of the dissipative solitons from their conservative counterparts is that they exist, as isolated attractors of the system, at a single value of the propagation constant, rather than continuous families parametrized by an arbitrary propagation constant [19]. In particular, as concerns GSs, 1D and 2D dissipative gap solitons in the complex Ginzburg-Landau equations with periodic potentials were reported in Ref. [20]. In this sense nonlinear \mathcal{PT} -symmetric systems, being not conservative and thus requiring the balance between dissipation and gain, but still allowing for existence of the continuous families of the solutions (what is the generic property of the such system provided the nonlinearity obey the same symmetry as the linear part [25]) occupy an intermediate position between the conservative and dissipative systems, and reduced to the former ones when the gain-loss coefficient becomes zero or the the later ones when appears disbalance between gain and loss.

The paper is organized as follows. The model is introduced in Sec. II. In Sec. III basic results are reported for soliton families found in the model, and the analysis of their stability, using both direct simulations and linearized equations for small perturbations, is presented in Sec. IV. The paper is concluded by Sec. V. Some special cases are separately considered in two Appendices.

II. THE MODEL

We consider the $\chi^{(2)}$ system, based on the evolution equations for the FF and SH components, $u_1(\zeta, \xi)$ and $u_2(\zeta, \xi)$, including the periodic \mathcal{PT} -symmetric potential, with an imaginary component of amplitude α , which is

assumed to act only onto the FF field:

$$i \frac{\partial u_1}{\partial \zeta} = \frac{\partial^2 u_1}{\partial \xi^2} + [V_1 \cos(2\xi) + i\alpha \sin(2\xi)] u_1 + 2u_1^* u_2, \quad (1a)$$

$$i \frac{\partial u_2}{\partial \zeta} = \frac{1}{2} \frac{\partial^2 u_2}{\partial \xi^2} + 2[V_2 \cos(2\xi) + q] u_2 + u_1^2. \quad (1b)$$

Here ζ and ξ are the propagation and transverse coordinates, q is the mismatch parameter, the $\chi^{(2)}$ coefficient is scaled to be 1, the asterisk stands for the complex conjugate, V_1 and V_2 are amplitudes of the real part of the periodic potential for the FF and SH components, while the period of the potential is set to be π by means of rescaling. Note that the conservative version of model (1), with $\alpha = 0$, was studied in Refs. [21, 22], where stable solitons were found.

The most straightforward situation, which corresponds to the periodic potential induced by a material grating etched into the $\chi^{(2)}$ waveguide, corresponds to $V_1 = V_2$ in Eqs. (1). Basic results are reported below for this situation. On the other hand, a *virtual grating* can be written in the waveguide by means of the electromagnetically-induced-transparency mechanism, see, e.g., Ref. [23]. In the latter case, the effective periodic potential is resonant, acting only in a narrow spectral interval. In this situation, it is reasonable to consider the system with $V_1 \neq 0$ and $V_2 = 0$, when the potential does not affect the SH field, which is far detuned from the resonance, and the opposite case, with $V_2 \neq 0$ and $V_1 = 0$. To illustrate similarities and differences between the different settings, some results for the systems with $V_2 = 0$ (the virtual grating) and $V_1 = V_2 = 0$ (the purely imaginary periodic potential) are presented in Appendices A and B, respectively. In the latter case, the GSs are completely unstable (as might be expected).

As concerns the loss and gain terms, they may be naturally assumed resonant (e.g., if both are induced by resonant dopants, with the inverted and uninverted populations in the gain and loss regions, respectively). For this reason, it is natural to assume that these terms are present only in the FF equation, as adopted in the system based on Eqs. (1). The opposite situation, with the imaginary potential acting on the SH field, is possible too; it will be considered elsewhere.

We look for localized solutions with propagation constant b in the form of

$$u_l(\xi, \zeta) = w_l(\xi) e^{ilb\zeta}, \quad l = 1, 2, \quad (2)$$

where complex functions $w_l(\xi)$ obey the stationary equations,

$$\frac{d^2 w_1}{d\xi^2} + [V_1 \cos(2\xi) + i\alpha \sin(2\xi) + b] w_1 + 2w_1^* w_2 = 0, \quad (3a)$$

$$\frac{1}{2} \frac{d^2 w_2}{d\xi^2} + 2[V_2 \cos(2\xi) + b + q] w_2 + w_1^2 = 0. \quad (3b)$$

Generally speaking, Eqs. (3) allow for solutions obeying one of the following symmetries: $\{w_1(\xi), w_2(\xi)\} = \{w_1^*(-\xi), w_2^*(-\xi)\}$ or $\{w_1(\xi), w_2(\xi)\} = \{-w_1^*(-\xi), w_2^*(-\xi)\}$. Note also that, in the well-known cascading limit, $|q| \rightarrow \infty$ [16], Eq. (3b) yields $w_2 \approx -w_1^2/(2q)$, and Eq. (3a) amounts to the equation with the cubic nonlinearity,

$$\frac{d^2 w_1}{d\xi^2} + [V_1 \cos(2\xi) + i\alpha \sin(2\xi) + b] w_1 - q^{-1} |w_1|^2 w_1 = 0. \quad (4)$$

As mentioned above, solitons in the \mathcal{PT} system based on Eq. (4) were recently studied in Refs. [8, 9].

III. GAP-SOLITON FAMILIES

It is well known that $\chi^{(2)}$ equations have particular solutions with the vanishing FF component, $w_1 \rightarrow 0$, while the SH part may either vanish or remain finite. These solutions are usually subject to the parametric instability [16], but they may be stabilized by an additional cubic nonlinearity [24], by an external trapping potential either [26], or by a \mathcal{PT} -symmetric localized defect [17].

To identify bifurcations which give rise to GSs from edges of bandgaps, it is also necessary to analyze the situation for $w_1 \rightarrow 0$. Generally speaking, one should then deal with three different cases [17], as shown below.

Case 1: both components are of the same order,

$$w_2 = \mathcal{O}(w_1), \quad w_1 \rightarrow 0. \quad (5)$$

Case 2: The SH field remains finite:

$$w_2 = \mathcal{O}(1), \quad w_1 \rightarrow 0. \quad (6)$$

Case 3: The SH amplitude scales as the square of the FF amplitude:

$$w_2 = \mathcal{O}(w_1^2), \quad w_1 \rightarrow 0. \quad (7)$$

Below, particular features of these three cases are considered separately.

A. Case 1

In the limit case defined as per condition (5), the nonlinear terms in both equations (3) can be neglected, which, at the leading order, results in the system of decoupled linear equations:

$$\frac{d^2 A_1}{d\xi^2} + [V_1 \cos(2\xi) + i\alpha \sin(2\xi) + b] A_1 = 0, \quad (8a)$$

$$\frac{d^2 A_2}{d\xi^2} + 4 [V_2 \cos(2\xi) + b + q] A_2 = 0. \quad (8b)$$

We notice that while Eq. (8b) is the well known Mathieu equation the linear spectral problem (8a) with the \mathcal{PT} -symmetric periodic potential was also thoroughly studied in literature [1, 6, 27]. In particular, it is known that subject to constraint $|\alpha| \leq V_1$, equation (8a) gives rise to the pure real spectrum. Now we turn to the *combined*

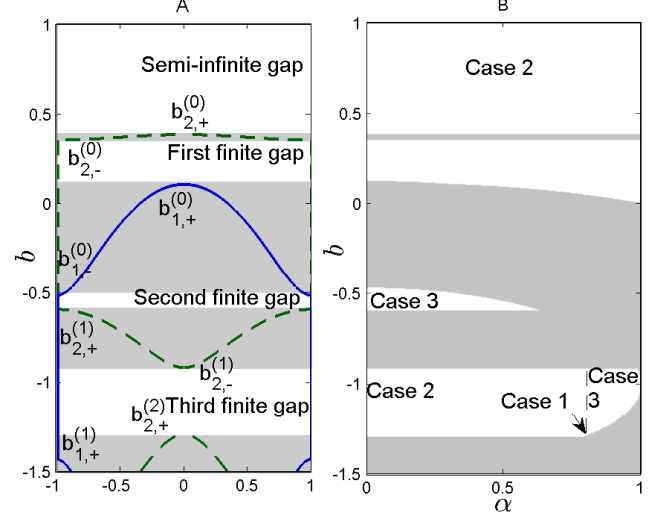


FIG. 1: (Color online) Panel A: the spectrum of potential (8) with $\alpha = 0.4$. The blue (solid) and green (dashed) curves correspond to the FF and SH components, respectively. Regions of FF- and SH-bands are shaded. The total gap correspond to white domains, as indicated in the figure. Panel B: Propagation constant *vs* the gain-loss coefficient. Edges of the total gap determined by the SH component are identifiable by horizontal lines, as they do not depend on α . The other edges are imposed by the FF component. The other parameters are $V_1 = V_2 = 1$ and $q = 0$.

bandgap spectrum of Eqs. (8), i.e. to the values of the propagation constant b which belong to the spectra of the both spectral problems. We denote by $b_{l,\pm}^{(m)}$ the propagation constant at the upper (+) or lower (-) edge of the m -th ($m = 0, 1, 2, \dots$) band for the FF ($l = 1$) and SH ($l = 2$) components, the latter being computed for $q = 0$ (then the band edges of the SH with $q \neq 0$ are given by $b_{2,\pm}^{(m)} - q$). Accordingly, the sequence of finite gaps is defined as $\Sigma_l^{(n)} = (b_{l,+}^{(n)}, b_{l,-}^{(n-1)})$, where $n = 1, 2, \dots$, and the semi-infinite gap is interval $\Sigma_l^{(0)} = (b_{l,+}^{(0)}, \infty)$. A *total gap* is the intersection of gaps of both components, as illustrated in panel A of Fig. 1.

Condition (5) implies that in Eqs. (8), b is a band edge for the FF and SH components simultaneously (this situation is illustrated in the right panel of Fig. 2). Since the band edges of the FF and the SH are in general independent, to let case (5) occur, and hence to let a branch bifurcate from the band edge $b_{1,\pm}^{(m)}$ of the FF, we have to impose the following condition,

$$b_{1,\sigma}^{(m)} = b_{2,\sigma}^{(m')} - q, \quad \sigma = \pm \quad (9)$$

where m' can be any band of the SH. Note, however, that only edges of the same type allow the existence of the bifurcation we are dealing with, which justifies the same sign, $+$ or $-$, on both sides of Eq. (9). Indeed, as one can see in panel A of Fig. 1, the individual gaps are located directly above (below) the band edges $b_{l,+}^{(m)}$ ($b_{l,-}^{(m)}$).

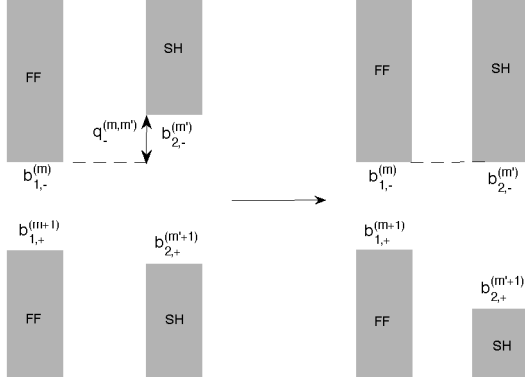


FIG. 2: A schematic diagram illustrating matching the band edges of the FF and SH for configuration of the Case 1. The left part of the figure represents the system without mismatch ($q = 0$). The arrow in the middle shows to what configuration the band structure is transferred when the mismatch $q = q_{-}^{(m,m')}$, resulting in the existence of the total gap, is imposed.

Once we impose condition (9), we force individual gaps to have at least one common edge. Then the total gap only exists if this edge is either the lower or upper one for the both bands simultaneously, as illustrated by Fig. 2.

Condition (9) imposes constraints on the design of the periodic structure. Typically, V_l would be fixed, and one could change the concentration of the dopant, which amounts to varying the amplitude of the imaginary part of the potential, α , or mismatch q . Accordingly, for given values values of $b_{1,\sigma}^{(m)}$ and $b_{2,\sigma}^{(m')}$, which are determined by the real part of the potential, it is possible to satisfy Eq. (9) by setting $q = q_{\sigma}^{(m,m')}$, where

$$q_{\sigma}^{(m,m')} = b_{1,\sigma}^{(m)} - b_{2,\sigma}^{(m')}, \quad \sigma = \pm. \quad (10)$$

All edges of the FF and the SH bands may be, in principle, matched with $q = q_{\sigma}^{(m,m')}$. Additionally it is possible to match the edges by tuning α alone, as can be seen in the third gap of panel B in Fig. 1 for $q = 0$. It is also possible to see that Case 1 in the semi-infinite gap cannot be realized solely through adjusting α .

1. Solitons in the semi-infinite gap

In Fig. 3, we display branches of the fundamental solitons, found numerically in the Case 1 in the semi-infinite

gap, using matching $q = q_{+}^{(0,0)}$. The branches are presented in the plane (b, P) , where $P = P_1 + P_2$, with $P_l \equiv l \int_{-\infty}^{\infty} |w_l|^2 d\xi$, ($l = 1, 2$), is the total power. Ex-

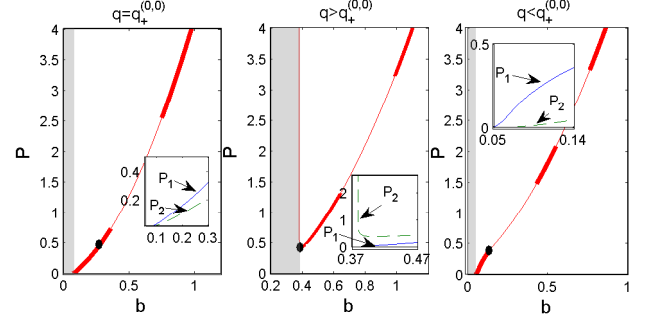


FIG. 3: (Color online) Branches of fundamental solitons for $\alpha = 0.7$ and different values of q , found in the semi-infinite gap. The left, central, and right panels correspond to cases 1, 2, and 3, with values $q = q_{+}^{(0,0)} = -0.316$, $q = 0$ and $q = -0.5134$ respectively [see Eqs. (5), (6), and (7)]. Insets show power components P_1 (line) and P_2 (dashed line) close to an edge of the semi-infinite total gap. Here and below, thick and thin lines represent stable and unstable solutions, respectively. Shaded regions denote bands of the FF and/or SH. Parameters are $V_1 = V_2 = 1$ and $\alpha = 0.7$.

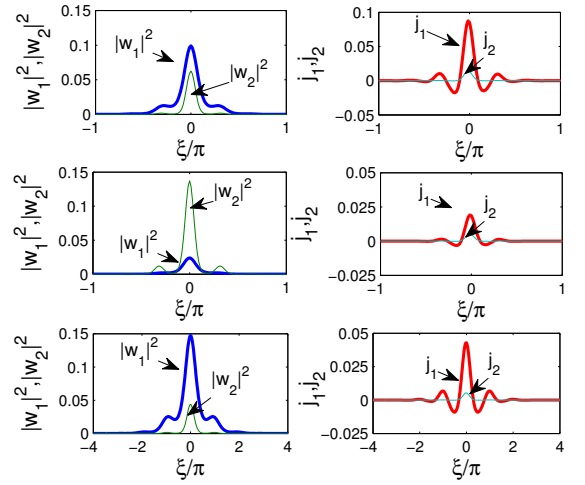


FIG. 4: (Color online) Examples of stable fundamental soliton solutions found in the semi-infinite gap pertaining to all the three cases, which are indicated by black circles in Fig. 3. The upper panels correspond to case 1, with $b = 0.25$ and band-edge matched with $q = q_{+}^{(0,0)} = -0.316$. The middle panels correspond to case 2, with $b = 0.43$ and $q = 0$. Lower panels show a solution of case 3 with $b = 0.21$ and $q = -0.5134$. The parameters are $V_1 = V_2 = 1$ and $\alpha = 0.7$.

amples of fundamental soliton solutions, i.e. the energy flows in each component as well as the currents are de-

fined as

$$j_l(\xi) = |w_l|^2 \frac{d\theta_l}{d\xi}, \quad \theta_l(\xi) = \arg w_l(\xi), \quad (11)$$

corresponding to the total power $P = 0.5$ are shown in Fig. 4. We observe, that while the currents having maximum in the center and domains with alternating sign, have very similar shapes of the spatial profiles, the power density is mainly concentrated in the FF and SH in the Cases 3 and 2, respectively and is approximately equally split between the two components in the Case 1 (as this is expected due to (5)). In all three cases the real valued FF current j_1 has a significantly higher amplitude than the current of the SH, j_2 , i.e. the balance between gain and losses is accomplished mainly due to the FF.

Here and in the rest of the paper, localized solutions satisfying zero boundary conditions were calculated numerically using a shooting method described in detail in Ref. [22] for the conservative case, $\alpha = 0$, and then extended to given $\alpha > 0$ by means of the Newton-Raphson method.

2. Solitons in the third finite gap

The main focus of this work is on the effects of the gain-loss coefficient α on branches of the fundamental solitons. To concentrate on this point, in what follows we set $q = 0$. For this choice it turns out possible to

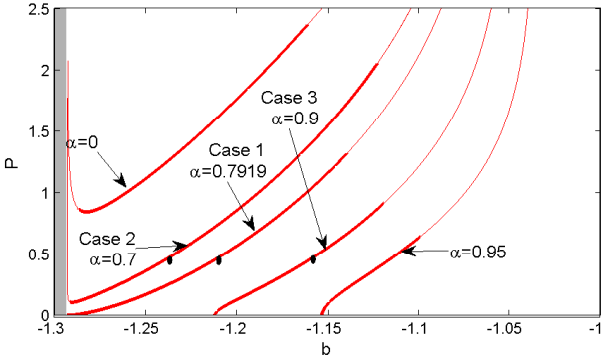


FIG. 5: (Color online) Branches of fundamental GSs found in the third finite gap for several values of amplitude α of the imaginary part of the periodic potential. All the three cases, 1, 2, and 3, which are defined as per Eqs. (5), (6), and (7), respectively, are presented. The gray region denotes the band of the SH component. The parameters are $V_1 = V_2 = 1$, $q = 0$.

obtain the matching condition $b_{1,+}^{(1)} = b_{2,+}^{(2)} = 1.29$ only in the third finite gap at $\alpha = 0.792$ (the value indicated by an arrow in Fig. 1B). In this context the consideration of the third gap becomes particularly relevant, as one can examine all three cases using only small deviations in parameter α . The respective modifications of the branches

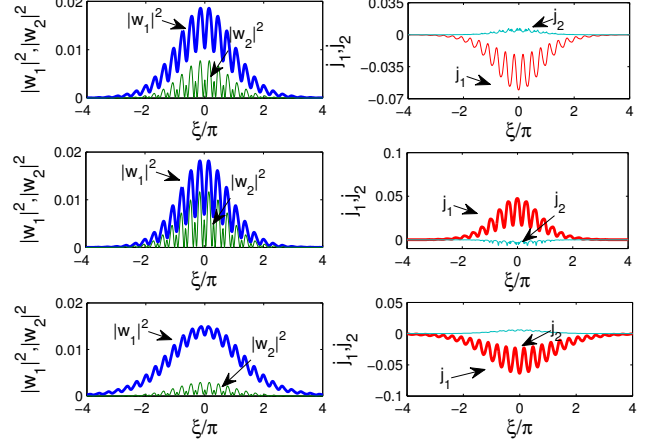


FIG. 6: (Color online) Examples of stable fundamental gap solitons in the third finite gap pertaining to all the three cases, which are indicated by black circles in Fig. 5. The upper panels corresponds to Case 1, with $b = -1.207$ and band-edge matched with $\alpha = 0.7919$. The middle panels correspond to Case 2, with $b = -1.234$ and $\alpha = 0.7$. Lower panels shows a solution of Case 3 with $b = 1.553$ and $\alpha = 0.9$. The total power of all the three solitons is $P = 0.5$. The parameters are $V_1 = V_2 = 1$, $q = 0$.

subject to variation of the amplitude of the imaginary part of the potential α are illustrated Fig. 5. Examples of the profiles of the respective gap solitons are shown in Fig. 6, where all three presented solutions have the same energy flow: $P = 0.5$. The most significant distinction with the situation observed in Fig. 4 for the solitons in the semi-infinite gap is that (i) now the intensity of the FF is always bigger than the intensity of the SH and (ii) the energy currents of the FF and SH are counter propagating and having constant signs (the current j_1 is negative while j_2 positive).

B. Stability analysis

The stability of the solutions found as outlined above was tested in direct simulations, as well as within the framework of the linear stability analysis. The later is based on the ansatz

$$u_l(\xi, \zeta) = \left(w_l + \delta_{l+} e^{-i\lambda\zeta} + \delta_{l-}^* e^{i\lambda^*\zeta} \right) e^{ilb\zeta}, \quad (12)$$

where $\delta_{l\pm}$ are amplitudes of small perturbations. The substitution of this ansatz into Eqs. (1) leads to the linear spectral problem,

$$L \begin{pmatrix} \delta_{2+} \\ \delta_{1+} \\ \delta_{2-} \\ \delta_{1-} \end{pmatrix} = \lambda \begin{pmatrix} \delta_{2+} \\ \delta_{1+} \\ \delta_{2-} \\ \delta_{1-} \end{pmatrix} \quad (13)$$

where

$$L = \begin{pmatrix} L_2 + 2b & 2w_1 & 0 & 0 \\ 2w_1^* & L_1 + b & 0 & 2w_2 \\ 0 & 0 & -L_2 - 2b & -2w_1^* \\ 0 & -2w_2^* & -2w_1 & -L_1^* - b \end{pmatrix}, \quad (14)$$

with

$$L_1 = \frac{d^2}{d\xi^2} + V_1 \cos(2\xi) + i\alpha \sin(2\xi), \quad (15a)$$

$$L_2 = \frac{1}{2} \frac{d^2}{d\xi^2} + 2[V_2 \cos(2\xi) + q]. \quad (15b)$$

Turning now to the stability properties of branches located in the semi-infinite gap, we obtain that the fundamental branches may have one or more instability intervals (see Fig. 3). The lengths of these intervals increase with α approaching the \mathcal{PT} -symmetry breaking point. This is a feature observed in all the cases considered below for semi-infinite gaps. In Fig. 7 we show examples of

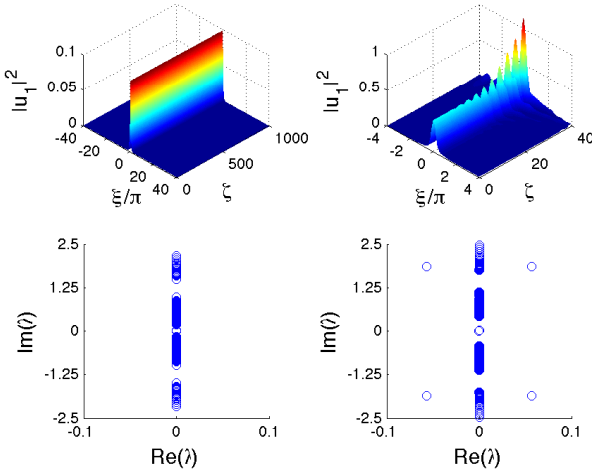


FIG. 7: (Color online) Top plots: The evolution of two GS solutions with 10% of amplitude random perturbations in Case 1 [see Eq. (5)] in the semi-infinite gap. Left panel has $b = 0.25$ and is stable. The right panel corresponds to unstable evolution of a solution with $b = 0.5$. The corresponding eigenvalues of small perturbations are shown in the lower panels. The parameters of the structure are $V_1 = V_2 = 1$, $\alpha = 0.7$ and $q = q_+^{(0,0)} = -0.316$.

the evolution of stable and unstable localized solutions. The observed oscillatory instability is due to a quartet of complex λ and instability develops as amplitude oscillations that increase with ζ .

Stability of the solitons of the fundamental branches in the third finite gap (Case 1 with $\alpha = 0.792$) is shown in Fig. 5. We observe an interval of stability which starts at the bifurcation point $b = b_{1,+}^{(1)} = b_{1,+}^{(2)} = 1.29$, the rest of the branch corresponding to unstable solutions.

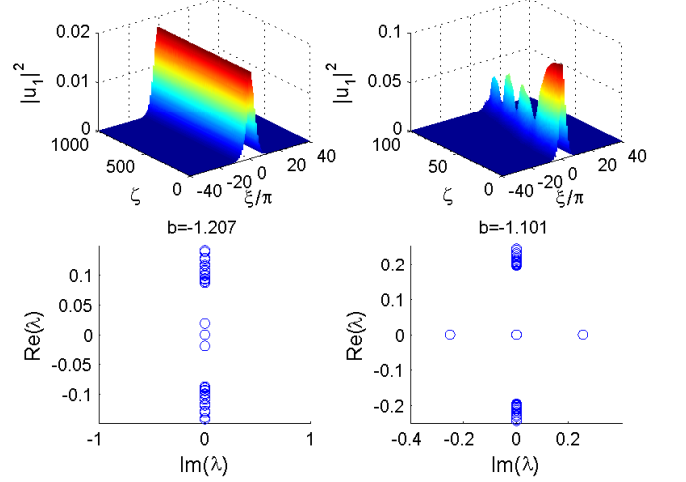


FIG. 8: (Color online) Top plots: The evolution of two GS solutions with 10% of amplitude random perturbations in Case 1 [see Eq. (5)] in the third finite gap. Left panel has $b = -1.207$ and is stable. The right panel corresponds to unstable evolution of a solution with $b = -1.101$. The corresponding eigenvalues of small perturbations are shown in the lower panels. The parameters of the structure are $V_1 = V_2 = 1$, $\alpha = 0.7919$ and $q = q_+^{(0,0)} = 0$.

Explicit examples of the direct propagation compared with the linear stability analysis are shown in Fig. 8. Stable and unstable GSs with slightly modified b belonging to the third finite gap are shown in the left and right columns, respectively. The two eigenvalues of the stable solution collide when b is varied and assume purely imaginary values. It can be seen in the upper right panel that the perturbed solution decays very rapidly.

C. Case 2

Now we turn to numerical studies of solutions satisfying condition (6), in the vicinity of the total gap, which coincides with an m -th SH gap edge, i.e. with $b_{2,\sigma}^{(m)}$. While FF component is vanishing in this case, i.e. $w_1 \rightarrow 0$ as $b \rightarrow b_{2,\sigma}^{(m)}$, the amplitude of the SH w_2 persists finite while its width increases (i.e. the SH in this limit becomes delocalized).

In particular, the effect of the delocalization is responsible for the grows of the total power, i.e. divergence of P , at $b \rightarrow b_{2,+}^{(0)}$ and $\alpha = 0.7$ shown in the central panel of Fig. 3 and at $b \rightarrow b_{2,+}^{(2)}$ shown in Fig. 5 for the branches with $\alpha = 0$ and $\alpha = 0.7$. Note that, in branches of Case 2 represented in Fig. 5 for both $\alpha = 0$ and $\alpha = 0.7$, P diverges at the same $b = b_{2,+}^{(2)}$, as the spectrum of Eq. (8b) is independent of α . Similar results for the conservative system, with $\alpha = 0$, were previously obtained

in Refs. [21, 22]. On the other hand, no delocalization of the SH component was observed for the branches satisfying condition (6) in Ref. [17], where a \mathcal{PT} -symmetric localized potential was considered, since the bifurcation of the second harmonic in that case departed from the localized defect state. The SH amplitude, we denote it

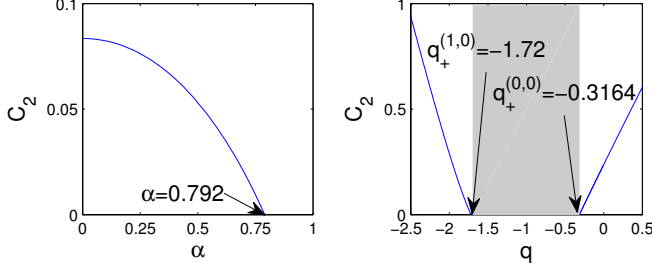


FIG. 9: Left panel: C_2 vs. α at the SH edge $b = b_{2,+}^{(1)} = -1.293$ of the third finite gap for $q = 0$. $C_2 = 0$ at $b_{1,+}^{(1)} = b_{2,+}^{(1)}$. Right panel: C_2 vs. q for $\alpha = 0.7$, at the edge $b = b_{2,+}^{(0)} = 0.3784$. The shaded region represents the interval where $b = b_{2,+}^{(0)} + q$ falls inside the band $[b_{1,-}^{(0)}, b_{1,+}^{(0)}]$. $C_2 = 0$ at $q = q_+^{(0,0)}$ and $q = q_+^{(1,0)}$. The parameters are $V_1 = V_2 = 1$.

by $C_2 = \max |w_2|$, of a solution with b close to $b_{2,\sigma}^{(m)}$, i.e., at $|b - b_{2,\sigma}^{(m)}| \ll 1$, depends on the phase mismatch and on the gain-loss coefficient.

This is illustrated in the left panel of Fig. 9, where we display plots C_2 vs. α , calculated at the SH edge $b = b_{2,+}^{(1)}$ which coincides with the edge of the third finite gap (like this is illustrated in the panel A of Fig. 1) for fixed $q = 0$. In the right panel of Fig. 9 we show dependence of C_2 on the mismatch q at the SH edge $b = b_{2,+}^{(0)}$ coinciding with the semi-infinite gap edge for fixed $\alpha = 0.7$. We found that $C_2 \rightarrow 0$ in the $C_2(\alpha)$ and $C_2(q)$ cases at specific value of the gain-loss coefficient: at $\alpha \approx 0.7919$ and $q = q_+^{(m,0)}$ respectively. In respect to values in which $C_2(q) \rightarrow 0$ we obtain this whenever q just adjusts the edge of the SH band-edge, which in the present analysis is $b = b_{2,+}^{(0)}$, to be located exactly of an edge of the FF of the same type (in the figure this means it is a edge of upper type, +), exactly as described by formula (10). In Fig. 9 we show only the values $q = q_+^{(0,0)}$ and $q = q_+^{(1,0)}$, which translates to the matching of edges $b_{1,+}^{(0)} = b_{2,+}^{(0)} + q_+^{(0,0)}$ and $b_{1,+}^{(1)} = b_{2,+}^{(0)} + q_+^{(1,0)}$. In respect to the left panel of Fig. 9, $C_2(\alpha)$ vanishes at the given value of the gain-loss coefficient corresponding to the situation when the edges of the FF and SH gaps coalesce (i.e. $b_{1,+}^{(1)} = b_{2,+}^{(2)}$).

Thus, whenever $C_2 \rightarrow 0$ is attained by a proper choice of α or q , both the FF and SH components emerge with infinitely small amplitudes $w_{1,2}$ when condition (9) is met, i.e., when Case 2 transforms in Case 1.

Examples of field profiles $w_{1,2}$ pertaining to the funda-

mental GS branches in the semi-infinite and in the third finite bandgap are displayed in middle panels of Figs. 4 and 6, respectively. In both figures the solutions are in the region close to the respective SH band edges $b_{2,+}^{(0)}$ and $b_{2,+}^{(1)}$ where (6) is satisfied.

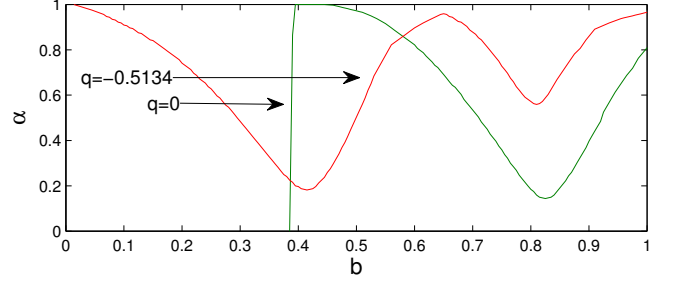


FIG. 10: (Color online) The boundary between stable (below the curves) and unstable (above the curves) gap-soliton solutions in the plane of (b, α) obtained from the linear-stability analysis. The curve with $q = 0$ represents a Case 2 branch bifurcating from $b_{2,+}^{(0)} = 0.3786$ and the curve with $q = -0.5134$ represents a Case 3 branch bifurcating from $b_{1,+}^{(0)}$. Note that while $b_{2,+}^{(0)}$ can be identified easily in the Case 2 curve as the point where the curve goes to $\alpha = 0$, $b_{1,+}^{(0)}$ is not fixed because it depends on α (See panel B of Fig. 1). The parameters are $V_1 = V_2 = 1$.

As concerns the stability of the GSs, Case 2 has one notable difference in the semi-infinite and in the third finite gaps in comparison with Case 1, whenever a given branch satisfying (6) bifurcates from a SH edge $b_{2,\sigma}^{(m)}$, a small unstable region close to $b_{2,\sigma}^{(m)}$ that persists even when $\alpha = 0$ exists. In Fig. 10 the curves separating stable and unstable solutions of the fundamental branch values of $q = 0$ and $q = -0.5134$ are shown in the plane (b, α) . The Case 2 branch is the curve with $q = 0$ in the semi-infinite gap, where can be seen stability threshold abruptly decays to zero. The other curve with $q = -0.5134$ a Case 1 bifurcation, it do not share this property. In both curves is possible to see that, as we reported in the previous section, there may be one or more unstable intervals with lengths that increase with α .

Examples of the propagation of stable and unstable solutions with variations in b in the semi-infinite gap are shown in Fig. 11. Instability appear due to the collision of internal modes with the band edges of the spectrum of (13) resulting in four complex eigenvalues λ . The propagation however shows that the perturbed solution can remain localized despite amplitude oscillations as is possible to see in the upper left panel of Fig. 11. At about $\zeta = 300$ there is an emission of energy from the localized field region but the structure quickly regains energy and remains localized. However not all linearly unstable solutions have this behaviour. In Fig. 12 we show an unstable solution that rapidly decays.

Examples of solutions in the third finite gap with

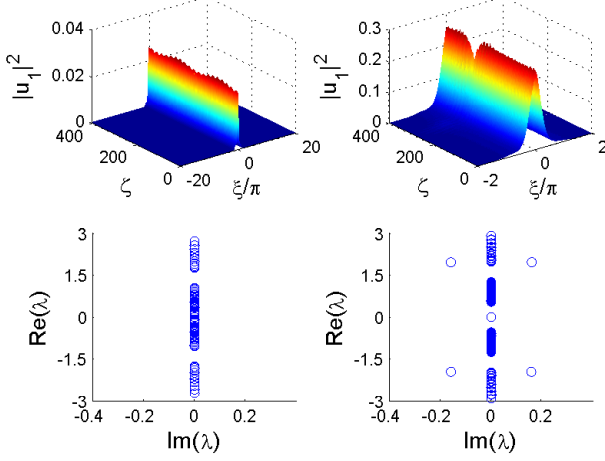


FIG. 11: (Color online) Top plots: The evolution of two GS solutions with 20% of amplitude random perturbations in Case 2 [see Eq. (6)] in the semi-infinite gap. Left panel has $b = 0.4$ and is stable. The right panel corresponds to unstable evolution of a solution with $b = 0.6$. Note that the linearly unstable solution remains localized. The corresponding eigenvalues of small perturbations are shown in the lower panels. The parameters of the structure are $V_1 = V_2 = 1$, $\alpha = 0.7$ and $q = 0$.

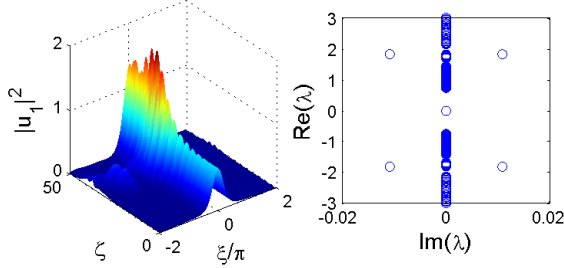


FIG. 12: (Color online) Left plot shows the evolution of an unstable localized solution with $b = 0.8$ added by 10% of amplitude random perturbations in Case 2 [see Eq. (6)] in the semi-infinite gap. The right plot shows the corresponding eigenvalues of small perturbations. The parameters of the structure are $V_1 = V_2 = 1$, $\alpha = 0.7$ and $q = 0$.

slightly different b are shown in Fig. 13. Unstable eigenvalue with positive λ appear when b is slightly bigger than $b = -1.268$ of the stable solution. Instability develops as a rapid increase of the amplitudes of the intensities $|w_{1,2}|^2$ with propagation.

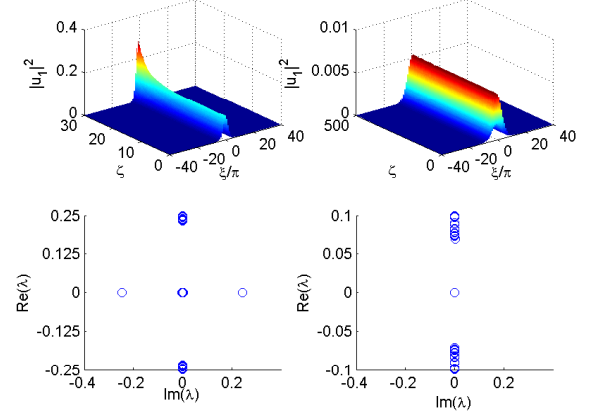


FIG. 13: (Color online) Top plots: The evolution of two GS solutions with 10% of amplitude random perturbations in Case 2 [see Eq. (6)] in the third finite gap. Left panel has $b = -1.11$ and is unstable. The right panel corresponds to stable evolution of a solution with $b = -1.268$. The corresponding eigenvalues of small perturbations are shown in the lower panels. The parameters of the structure are $V_1 = V_2 = 1$, $\alpha = 0.7$ and $q = 0$.

D. Case 3

Finally, we consider GS branches generated by bifurcations which obey condition (7) satisfied in a vicinity of the FF edge of the total gap, $b = b_{1,\sigma}^{(m)}$. The branch

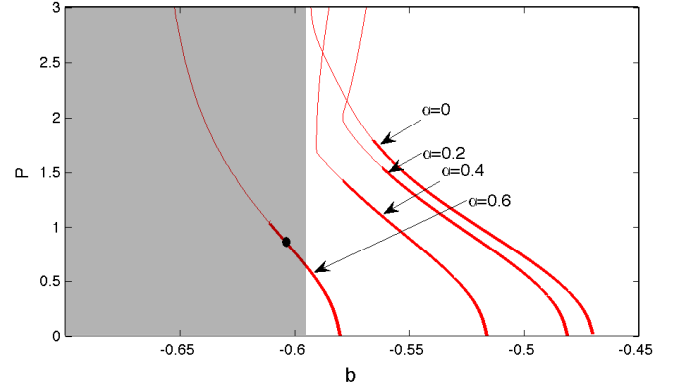


FIG. 14: (Color online) Branches of fundamental GSs for several values of α in the second finite gap. The bifurcations are of the Case 3 type. The shaded region denotes the band of the SH component. The branches extend into the SH band, as *embedded solitons*, at $\alpha > 0.41$. Thick and thin lines represent stable and unstable solutions, respectively. The parameters are $V_1 = V_2 = 1$, $q = 0$.

of the fundamental GS solutions pertaining to Case 3 is displayed in the right panel of Fig. 3 for the semi-infinite gap.

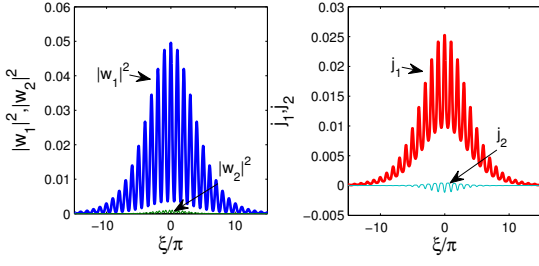


FIG. 15: (Color online) An example of a stable *embedded soliton* with $b = -0.6$, indicated by the black circle in Fig. 14 inside the SH band. This solution belongs to the branch of fundamental solitons that bifurcates from $b_{1,-}^{(0)}$ in the second finite gap. The parameters are $\alpha = 0.6$, $V_1 = V_2 = 1$ and $q = 0$.

An example of GS solution is displayed in the lower panels Fig. 4. It can be seen that $|w_1|^2$ has a much higher amplitude than $|w_2|^2$. Fundamental branches of Case 3 are also represented by the branches with $\alpha = 0.9$ and $\alpha = 0.95$ in Fig. 5 for the third gap. An example of the respective field profiles for the GS branch in the third finite bandgap, bifurcating from $b_{1,+}^{(1)}$, is shown in the lower panels of Fig. 6. Also in the same figure, can be noted that while $|w_1|^2$ is strictly positive, j_1 is strictly negative. The current j_2 is strictly positive.

We observe in Fig. 14, where branches for several values of α are found in the second finite gap, that the branch which bifurcates from $b_{1,+}^{(0)}$ at $\alpha = 0.6$ goes into the band of the SH, where it becomes a family of *embedded solitons* (ESs) [28, 29], i.e., those existing inside (*embedded into*) the continuous spectrum. The existence of such solitons is explained by fact that their decaying asymptotic tails at $|\xi| \rightarrow \infty$ follow relation (7), hence the SH equation is *non-linearizable* for the decaying tails, invalidating the standard argument for the non-existence of solitons whose propagation constant falls into the band. We have found that the GS branches extend into the SH band for $\alpha > 0.41$. In Fig. 15 we show a typical example of stable ES. In particular is possible to see that both $|w_{1,2}|^2$ decay rapidly despite being in the SH band.

Note that no ESs were found for the conservative version of the present system, with $\alpha = 0$ [21, 22]. Embedded solitons were found in Ref. [29] in the conservative model without the potential ($V_1 = V_2 = 0$), but with cubic nonlinear terms added to the equations, otherwise only *quasi-solitons* can be found, with non-vanishing tails at $|\xi| \rightarrow \infty$ [30]. Furthermore, in the conservative system the ESs were found only at discrete values of b . A noteworthy feature of ESs in the present system is that a part of their family is stable, as seen in Fig. 14 and in the left panels of in Fig. 16 while in the conservative system the isolated ES is *semi-stable* (in Ref. [29], the ES was stable against perturbations that increased the total power, but unstable against those which decreased it). The unstable perturbations in the semi-stable con-

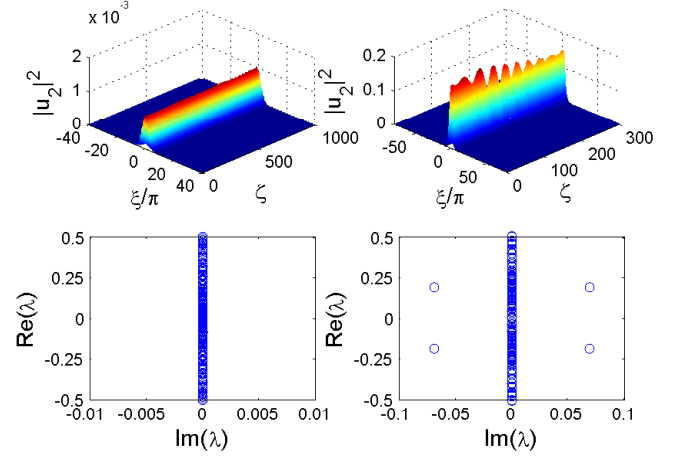


FIG. 16: (Color online) Top plots: The evolution of two GS solutions with 10% of amplitude random perturbations in Case 3 [see Eq. (7)] in the second finite gap. Left panel has $b = -0.6$ and is stable. The right panel corresponds to unstable evolution of a solution with $b = -0.65$. The corresponding eigenvalues of small perturbations are shown in the lower panels. The parameters of the structure are $V_1 = V_2 = 1$, $\alpha = 0.6$ and $q = 0$.

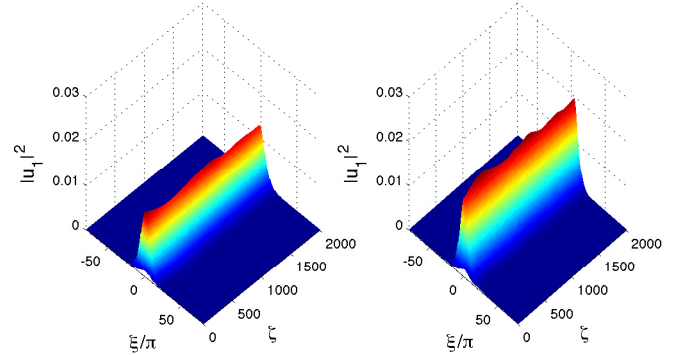


FIG. 17: (Color online) An example of the stable evolution of the GS with $b = -0.6$, indicated by the black circle in Fig. 14, inside the SH band pertaining to the fundamental branch that bifurcates from $b_{1,+}^{(1)}$, in the third finite gap. In the left panel the initial condition is $u_{1,2}(\xi, 0) = 0.95 \cdot w_{1,2}(\xi)$ and in the right panel it is $u_{1,2}(\xi, 0) = 1.05 \cdot w_{1,2}(\xi)$. In both cases, the soliton is stable. The parameters are $\alpha = 0.6$, $V_1 = V_2 = 1$ and $q = 0$.

servative system grow *sub-exponentially* [in fact, as ζ^2 , rather than as $\exp(\text{const} \cdot \zeta)$]. In our system, the gain component supplies the power and helps to stabilize perturbed solitons, see Fig. 17. Instability, when it appears, is due to the emergence of quartets of complex eigenvalues, as is possible to see in the right panels of Fig. 16. The propagation of perturbed unstable solution revealed that the decay is oscillatory. We also mention that in

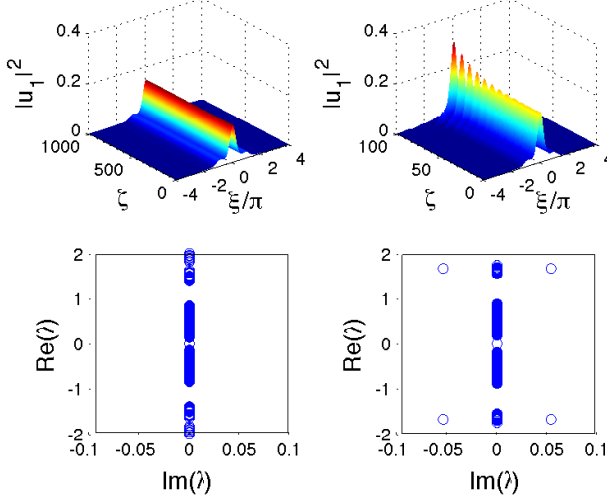


FIG. 18: (Color online) Top plots: The evolution of two GS solutions with 10% of amplitude random perturbations in Case 3 [see Eq. (7)] in the semi-infinite gap. Left panel has $b = 0.21$ and is stable. The right panel corresponds to unstable evolution of a solution with $b = 0.25$. Note that the linearly unstable solution remains localized. The corresponding eigenvalues of small perturbations are shown in the lower panels. The parameters of the structure are $V_1 = V_2 = 1$, $\alpha = 0.7$ and $q = -0.5134$.

Ref. [31] continuous families of ESs in a system with a cubic nonlinearity were found for moving solitons in the plane of (v, b) , where v is the soliton's velocity. However, the ES solutions still formed discrete sets for any given v , including the case of the quiescent solitons, $v = 0$, considered here. To the best of our knowledge, the present system furnishes the first example a continuous branch of ESs in a system with a purely quadratic nonlinearity, a part of the branch being stable. In the semi-infinite gap, the behavior of solitons in Case 3 is similar to that in Case 1, outlined above, with one or more alternating stable and unstable intervals, whose lengths depend on the gain-loss strength, α . In Fig. 18 we show examples of stable and unstable evolutions in the semi-infinite gap. The linear stability analysis shows four complex eigenvalues in the case of the unstable solution. Dynamics shows that instability develops as increasing amplitude oscillations.

In all the finite gaps, we have found two regions, one stable, starting at the bifurcation point, and the other unstable, as one can see in Fig. 3 for values $\alpha = 0.9$ and $\alpha = 0.95$ and Fig. 14. In Fig. 19 we show examples of stable and unstable solutions in the second-finite gap. The linear stability analysis shows that in the unstable solution the eigenvalues responsible for the instability are purely real. Dynamics shows that the amplitude of the perturbed unstable solution grows without oscillations.

Lastly, stable solutions have never been found for $|\alpha| >$

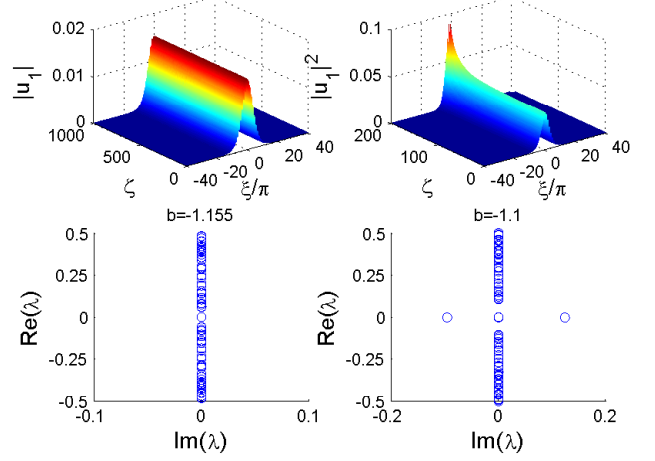


FIG. 19: (Color online) Top plots: The evolution of two GS solutions with 20% of amplitude random perturbations in Case 3 [see Eq. (7)] in the second finite gap. Left panel has $b = -1.155$ and is stable. The right panel corresponds to unstable evolution of a solution with $b = -1.1$. Note that the linearly unstable solution remains localized. The corresponding eigenvalues of small perturbations are shown in the lower panels. The parameters of the structure are $V_1 = V_2 = 1$, $\alpha = 0.9$ and $q = 0$.

V_1 . This conclusion is qualitatively similar to that made in other nonlinear \mathcal{PT} systems, where solitons do not exist above a critical level of the gain-loss coefficient [8, 10].

IV. CONCLUSION

In this work we have introduced the model combining the linear \mathcal{PT} -symmetric part and the $\chi^{(2)}$ nonlinearity. The \mathcal{PT} terms are represented by the complex potential acting on the FF (fundamental-frequency) component, whose imaginary part, accounting for the spatially separated and mutually balanced gain and loss, is, as usual, the odd function of the coordinate. The potential acting on the SH (second-harmonic) wave is assumed to be purely real. The complex linear potential gives rise to the corresponding bandgap spectrum. Solutions for solitons were looked for in the semi-infinite and finite gaps, starting from the bifurcation which gives rise to such solitons at edges of the respective gap. Families of the solitons have been thus constructed, and their stability was investigated by means of the linearization and direct simulations alike. While the system contains several parameters, we have primarily focused on effects produced by the variation of the amplitude of the imaginary part of the potential, which is specific to the \mathcal{PT} -symmetric system. A noteworthy result is that the present system may support of continuous family of solitons embedded into the continuous spectrum of the SH component, and a part of

the family of such embedded solitons is stable. The analysis has been reported, chiefly, for the most physically relevant case of equal effective amplitudes of the real potentials acting on the FF and SH waves. In addition, a more exotic case of the real potential acting solely on the FF component was investigated too (in Appendix A).

A natural extension of this analysis may be performed for the two-dimensional version of the $\chi^{(2)}$ system with the \mathcal{PT} -symmetric periodic potential. In that case, it may be also interesting to construct vortex solitons, in addition to the fundamental ones, and investigate their stability.

V. ACKNOWLEDGMENTS

V.V.K. acknowledge support of the Fundação para a Ciência e a Tecnologia (Portugal) under the grants PTDC/FIS/112624/2009 and PEst-OE/FIS/UI0618/2011. F. C. M. was partially supported by Alban fellowship No. E06D100918BR.

Appendix A: The system with the "virtual grating"

Here we consider the case of $V_2 = 0$, i.e. the periodic potential acting only on the FF component. A typical

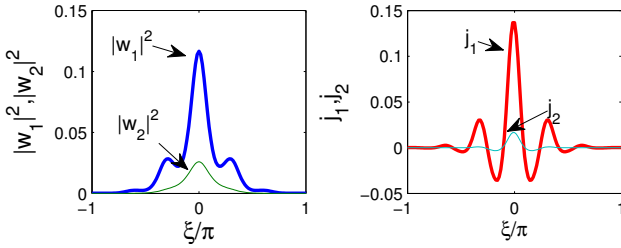


FIG. 20: (Color online) The intensities $|w_{1,2}|^2$ and currents $j_{1,2}$ of a stable GS solution with propagation constant $b = 0.2$ pertaining to the semi-infinite gap. The parameters of the system are $V_1 = 1$, $V_2 = 0$, $q = 0$ and $\alpha = 0.9$.

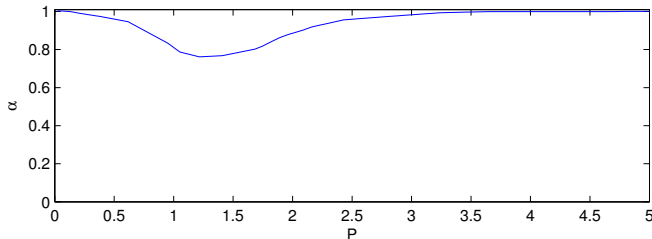


FIG. 21: (Color online) The stability boundary in the plane of (P, α) , in the system with $V_1 = 1$ and $V_2 = 0$. The instability area is located above the boundary.

example of a stable GS, found as solutions to Eqs. (3a) and (3b) in the absence of the periodic potential acting on the SH, is displayed in Fig. 20. It is seen that its shape is conspicuously different from that of the solitons found above in the system with $V_2 = V_1$, cf. Fig. 6.

The analysis of the stability of solitons in Eqs. (1a) and (1b) in the case of $V_2 = 0$ reveals a stability boundary, shown in in Fig. 21, which is qualitatively similar to its counterparts presented above for the system with $V_2 = V_1$, cf. Fig. 10. In particular, the instability area appears for values of α above a certain threshold. However, the difference is that only one instability interval exists in this case, and the threshold for its appearance, $\alpha \approx 0.75$, is higher than in the system where the periodic potential acts on both components.

Appendix B: The case of a purely imaginary potential

Here we consider the limit case of the system when the potential in Eq. (1a) is purely imaginary, and no potential appears in Eq. (1b), i.e., $V_1 = V_2 = 0$. A

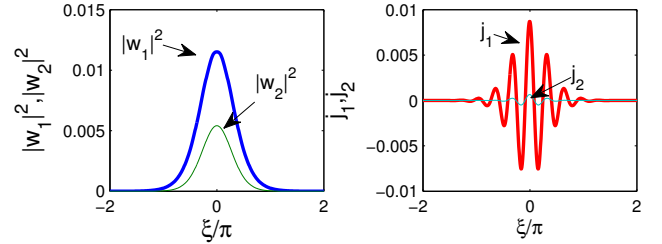


FIG. 22: (color online) The intensities $|w_{1,2}|^2$ and currents $j_{1,2}$ of a GS with $b = 0.06$, in the system with $V_1 = V_2 = 0$ (no real potential) and $q = 0$, $\alpha = 0.5$.

typical example of the soliton found in this case is shown in Fig. 22.

In this case, all the solitons are unstable at $\alpha > 0$. The respective instability growth rate being rather small, Fig. 23 shows that the growth of the instability in direct simulations starts abruptly, as the instability eigenvalues are purely imaginary, see Eq. (12).

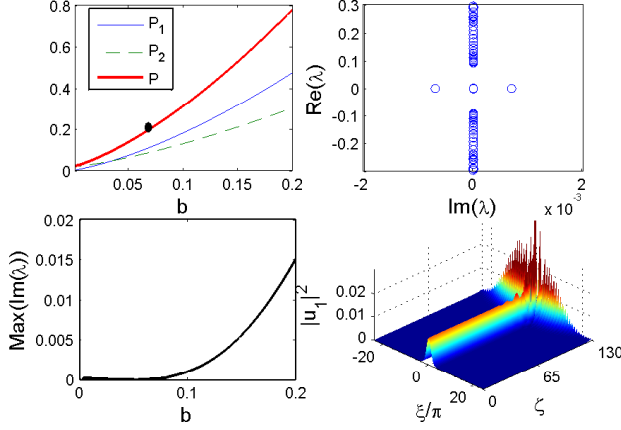


FIG. 23: (Color online) Solitons in the system with $V_1 = V_2 = q = 0$ and $\alpha = 0.5$. The upper left panel: The power-vs.-propagation-constant (b) branch. The lower left panel: The instability eigenvalue, λ , with the largest imaginary part, as a function of b . The upper right panel: Stability eigenvalues for the soliton with $b = 0.06$, the instability being accounted for by a pair of small purely imaginary eigenvalues. The lower right panel: The unstable propagation of the soliton randomly perturbed at the 1% amplitude level.

-
- [1] C. M. Bender, Rep. Prog. Phys. **70**, 947 (2007).
[2] See special issues: H. Geyer, D. Heiss, and M. Znojil, Eds., J. Phys. A: Math. Gen. **39**, *Special Issue Dedicated to the Physics of Non-Hermitian Operators (PHHQP IV)* (University of Stellenbosch, South Africa, 2005) (2006); A. Fring, H. Jones, and M. Znojil, Eds., J. Math. Phys. A: Math. Theor. **41**, *Papers Dedicated to the Subject of the 6th International Workshop on Pseudo-Hermitian Hamiltonians in Quantum Physics (PHHQPVI)* (City University London, UK, 2007) (2008); C. Bender, A. Fring, U. Günther, and H. Jones, Eds., *Special Issue: Quantum Physics with non-Hermitian Operators*, J. Math. Phys. A: Math. Theor. **41**, No. 44 (2012).
[3] A. Mostafazadeh, J. Math. Phys. A: Math. Gen. **36**, 7081 (2003).
[4] A. Ruschhaupt, F. Delgado, and J. G. Muga, J. Phys. A: Math. Gen. **38**, L171 (2005).
[5] C. E. Rüter, K. G. Makris, R. El-Ganainy, D. N. Christodoulides, M. Segev, and D. Kip, Nature Phys. **6**, 192 (2010).
[6] K. G. Makris, R. El-Ganainy, D. N. Christodoulides, and Z. H. Musslimani, Phys. Rev. Lett. **100**, 103904 (2008); S. Longhi, Phys. Rev. A **81**, 022102 (2010).
[7] K. G. Makris, R. El-Ganainy, D. N. Christodoulides, and Z. H. Musslimani, Int. J. Theor. Phys. **50**, 1019 (2011).
[8] Z. H. Musslimani, K. G. Makris, R. El-Ganainy, and D. N. Christodoulides, Phys. Rev. Lett. **100**, 030402 (2008); Z. Lin, H. Ramezani, T. Eichelkraut, T. Kottos, H. Cao, and D. N. Christodoulides, Phys. Rev. Lett. **106**, 213901 (2011); X. Zhu, H. Wang, L.-X. Zheng, H. Li, and Y.-J. He, Opt. Lett. **36**, 2680 (2011); C. Li, H. Liu, and L. Dong, Opt. Exp. **20**, 16823 (2012).
[9] S. Nixon, L. Ge, and J. Yang, Phys. Rev. A **85**, 023822 (2012).
[10] R. Driben and B. A. Malomed, Opt. Lett. **36**, 4323 (2011); EPL **96**, 51001 (2011); EPL **99**, 54001 (2012); F. K. Abdullaev, V.V. Konotop, M. Ögren, and M.P. Sørensen, Opt. Lett. **36**, 4566 (2011); N. V. Alexeeva, I. V. Barashenkov, A. A. Sukhorukov, and Y. S. Kivshar, Phys. Rev. A **85**, 063837 (2012).
[11] S. V. Dmitriev, A. A. Sukhorukov, and Y. S. Kivshar, Opt. Lett. **35**, 2976 (2010); S. V. Suchkov, B. A. Malomed, S. V. Dmitriev, and Y. S. Kivshar, Phys. Rev. E **84**, 046609 (2011).
[12] V. V. Konotop, D. E. Pelinovsky, and D. A. Zezyulin, arXiv:1210.2216 [nlin.PS]
[13] F. Kh. Abdullaev, Y. V. Kartashov, V. V. Konotop, and D. A. Zezyulin, Phys. Rev. A **83**, 041805(R) (2011); D. A. Zezyulin, Y. V. Kartashov, V. V. Konotop, Europhys. Lett. **96**, 64003 (2011); A. E. Miroshnichenko, B. A. Malomed, and Y. S. Kivshar, Phys. Rev. A **84**, 012123 (2011).
[14] D. A. Zezyulin and V. V. Konotop, Phys. Rev. A **85**, 043840 (2012).
[15] Y. He, X. Zhu, D. Mihalache, J. Liu, and Z. Chen, Phys. Rev. A **85**, 013831 (2012); Opt. Commun. **285**, 3320 (2012);
[16] G. I. Stegeman, D. J. Hagan, L. Torner, Opt. Quant. Electr. **28**, 1691 (1996); C. Etrich, F. Lederer, B. A. Malomed, T. Peschel, and U. Peschel, Prog. Opt. **41**, 483 (2000); A. V. Buryak, P. Di Trapani, D. V. Skryabin, and S. Trillo, Phys. Rep. **370**, 63 (2002).

- [17] F. C. Moreira, F. Kh. Abdullaev, V. V. Konotop, and A. V. Yulin, Phys. Rev. A **86**, 053815 (2012)
- [18] J. Yang, *Nonlinear Waves in Integrable and Nonintegrable Systems* (SIAM: Philadelphia, 2010).
- [19] B. A. Malomed, Physica D **29**, 155 (1987); S. Fauve and O. Thual, Phys. Rev. Lett. **64**, 282 (1990).
- [20] H. Sakaguchi and B. A. Malomed, Phys. Rev. E **77**, 056606 (2008); Phys. Rev. E **80**, 026606 (2009).
- [21] Y. V. Kartashov, L. Torner and V. Vysloukh, Opt. Lett. **29** 1117- (2004), V. A. Brazhnyi, V. V. Konotop, S. Coulibaly, and M. Taki, Chaos **17**, 037111 (2007);
- [22] F. C. Moreira, F. Kh. Abdullaev, and V. V. Konotop, Phys. Rev. A **85** 023843 (2012).
- [23] Y. Li, B. A. Malomed, M. Feng, and J. Zhou, Phys. Rev. A **83**, 053832 (2011).
- [24] A. V. Buryak, Y. S. Kivshar, and S. Trillo, Opt. Lett. **20**, 1961 (1995).
- [25] D. A. Zezyulin and V.V. Konotop, Phys. Rev. Lett. **108**, 213906 (2012)
- [26] H. Sakaguchi and B. A. Malomed, J. Opt. Soc. Am. B **29**, 2741 (2012).
- [27] B. Midya, B. Roy, and R. Roychoudhury, Phys. Lett. A **374**, 2605 (2010); E.-M. Graefe and H. F. Jones, Phys. Rev. A **84**, 013818 (2011).
- [28] J. Yang, B. A. Malomed, and D. J. Kaup, Phys. Rev. Lett. **83**, 1958-1961 (1999).
- [29] J. Yang, B. A. Malomed, D. J. Kaup and A. R. Champneys, Math. Comp. Sim. **56**, 585-600 (2001).
- [30] B. A. Malomed, D. J. Kaup, and R. A. Van Gorder, Phys. Rev. E **85**, 026604 (2012).
- [31] J. Yang and T. R. Akylas, Stud. Appl. Math. **111**, 359-375 (2003)